Effects of quicklime application rate on carbon mineralization in strongly acidic soil of Cunninghamia lanceolata plantations

Zhang Jiayi
Tong Jiacheng
Fang Fang
Zhang Yanting
Li Songzhe
Ma Dandan
Shunbao Lu
luxunbao8012@126.com

Jiangxi Normal University https://orcid.org/0000-0002-8578-4734
Zhang Yanjie

Research Article

Keywords: Strongly acidic soil, Quicklime amendment, Carbon mineralization, Microbial biomass, Extracellular enzyme activity, PLS-SEM

Posted Date: June 12th, 2026

DOI: https://doi.org/10.21203/rs.3.rs-9605588/v1

Abstract

Aims

Strongly acidic Chinese fir (*Cunninghamia lanceolata*) plantation soils face significant constraints in nutrient and carbon dynamics. This study aimed to investigate the biogeochemical mechanisms governing carbon cycling in these soils under varying quicklime amendment rates.

Methods

Soils collected from Chinese fir plantations treated with six quicklime amendment rates (0–3,000 kg hm^{-2}), and incubated for 49 days in carbon mineralization experiment. The analyses integrated high-throughput sequencing, PICRUSt2 functional prediction, Mantel tests, and partial least squares structural equation modeling (PLS-SEM) to evaluate the relationships among soil physicochemical properties, microbial communities, and carbon mineralization.

Results

Quicklime amendment exerted significant nonlinear, dose-dependent effects on soil carbon cycling, with 2,250 kg hm^{-2} (T4) identified as the optimal threshold, whereas excessive application (3,000 kg hm^{-2}) produced significant inhibitory effects ($P < 0.05$). Key mechanistic insights reveal that optimal quicklime application: (i) Alleviates acidity stress by increasing soil pH from 4.71 to 5.25, thereby increasing microbial biomass carbon and phosphorus by 113.96% and 192.75%, respectively; (ii) Elevates β-glucosidase and cellobiohydrolase activities ($P < 0.05$) to drive an 88.5% increase in cumulative carbon mineralization, while exhibiting a decoupling between high enzymatic capacity and lower functional gene abundance indicative of a high-efficiency metabolic strategy; (iii) Drives carbon mineralization through a sequential mediation pathway (PLS-SEM GoF = 0.519) where improved physicochemical properties promote microbial biomass accumulation (path coefficient = 0.860), which subsequently enhances extracellular enzyme activity (path coefficient = 0.899). Notably, microbial biomass magnitude (0.899) rather than community composition (0.074) was the primary regulator of enzymatic capacity, with nitrate nitrogen acting as a key factor linking environmental conditions to microbial functional profiles.

Conclusion

Optimal quicklime application ameliorates physicochemical constraints and stimulates microbial biomass growth, thereby enhancing extracellular enzyme-mediated organic carbon decomposition in acidic Chinese fir plantation soils. These findings highlight that microbial biomass magnitude, rather than community structure, is the primary driver of enzymatic capacity, providing a scientific basis for optimizing carbon cycling management in acidic forest soils.

Introduction

Chinese fir *(Cunninghamia lanceolata)* is the dominant plantation tree species in southern China. Due to long-term successive rotations and irrational management practices, soil acidification in plantation stands has become increasingly severe (Błońska et al. 2016; Selvaraj et al. 2017; Wang et al. 2011). Strongly acidic conditions (pH < 5.0) not only restrict soil nutrient availability and significantly suppress microbial activity and extracellular enzyme secretion, but also directly impair soil organic carbon (SOC) mineralization and sequestration processes, thereby seriously constraining the productivity and sustainability of plantation ecosystems (He et al. 2025; Lei et al. 2026; Li et al. 2025).

Quick lime (CaO), as a fast-acting soil amendment, has been widely applied to neutralize soil acidity (Fageria and Baligar 2008; Jouichat and Khiari 2026). Previous studies have confirmed that quicklime application can rapidly elevate soil pH and replenish calcium (Ca) levels (Ahmad et al. 2014; Ismail et al. 2026; Jouichat et al. 2024). Nevertheless, significant knowledge gaps remain regarding the complex mechanisms through which quicklime addition influences carbon cycling in forest soils. First, dramatic shifts in pH may disrupt the existing microbial community equilibrium, alter carbon source utilization strategies, and consequently induce non-linear fluctuations in SOC mineralization rates (Ahmad et al. 2014; Grover et al. 2017; Holland et al. 2018). Furthermore, we still lack a systematic quantitative assessment of whether excessive quicklime application suppresses microbial metabolic functions through elevated Ca^{2+} concentrations, revealing a possible threshold effect (Rowley et al. 2018; Yang et al. 2026). More critically, the mechanisms by which alterations in soil physicochemical properties drive microbial community structural reorganization, functional gene expression, and enzyme activity changes, ultimately feeding back into carbon mineralization still awaits a systematic explanation.

To address these issues, this study established a gradient of quicklime addition treatments in a strongly acidic Chinese fir plantation soil, followed by soil collection for laboratory incubation to assess carbon mineralization dynamics, coupled with soil enzymology analyses and high-throughput sequencing to characterize shifts in physicochemical properties, microbial community structure, and functional gene abundance. The analysis aimed to identify mechanisms through which quicklime addition alters soil carbon turnover. Three questions guided the inquiry. The first question asked whether carbon mineralization exhibits a dose dependent response to quicklime that would indicate an amendment threshold. The second question investigated how microbial community reassembly shifts carbon metabolism from a pattern of proliferation toward one of efficiency. The third question employed partial least squares structural equation modeling (PLS-SEM) to estimate the contributions of soil physicochemical properties, microbial community structure, and extracellular enzyme activities to carbon mineralization. These results offer a scientific basis for soil restoration and carbon management in degraded Chinese fir plantations.

Materials and methods

Study site description

The study site is located in Dongshan Village, Xiangshan Town, Chongren County, Fuzhou City, Jiangxi Province, China (116°05'-116°06'E, 27°45'-27°46'N). The experimental area lies at elevations of 200–500 m and experiences a humid subtropical monsoon climate. The terrain consists predominantly of hills and supports diverse soil types. Mean annual precipitation is approximately 1,600 mm, primarily concentrated between April and September. Sunshine duration reaches approximately 1,700 hours per year, and the frost-free period extends to 270 days. Mean annual temperature is approximately 17°C. July temperatures peak at 36°C, while January lows drop to -2°C.

Plot establishment

In September 2021, we selected representative Chinese fir plantations at Dongshanling, Xiangshan Town, Chongren County, Fuzhou City, Jiangxi Province, and established three fixed plots as replicates, maintaining an inter-plot spacing of no less than 5 m. Within each plot, six fixed subplots of 5 m × 5 m were established. To differentiate the effects of varying amendment doses on soil component respiration, roots within the subplots were severed using the trenching method. PVC barriers were subsequently inserted into the trenches, and the excavated soil was backfilled, to prevent root ingrowth. Gradient quicklime additions were randomly assigned to each subplot. From 2021 onward, fertilization and aqueous solution spraying operations were conducted in September of each year and March of the following year. The six treatment levels of quicklime addition were as follows: CK: 0 kg hm^{-2}, T1: 375 kg hm^{-2}, T2: 750 kg hm^{-2}, T3: 1,500 kg hm^{-2}, T4: 2,250 kg hm^{-2}, and T5: 3,000 kg hm^{-2}.

Sample collection and processing

In September 2024, aboveground plant parts and litter were cleared from subplot. Within each subplot, five sampling points were selected in an S-shaped pattern. Surface soil at a depth of 0–20 cm was collected using a soil auger with a diameter of 7.5 cm, and the five subsamples were thoroughly mixed to form a composite sample. A total of 18 samples were collected from the three plots. After collection, soil samples were passed through a 2 mm sieve and divided into three portions of approximately 1 kg each. Every portion was labeled, placed in a No. 8 sterile resealable bag, and transported to the laboratory. One portion was air-dried for determination of soil physicochemical properties; one portion was stored at -80°C for bacterial high-throughput sequencing; and the remaining portion was stored at 4°C for soil enzyme activity determination and future use.

Analytical methods

Determination of soil biochemical indicators: Soil pH was measured using a pH meter at a soil-to-water ratio of 1:2.5. Soil organic carbon (SOC) was determined by the low-temperature external heating potassium dichromate oxidation–spectrophotometric method (Nelson and Sommers 1996). Total nitrogen (TN) was determined by the Kjeldahl method (Bremner 1996). Total phosphorus (TP) was determined by the molybdenum–antimony–ascorbic acid colorimetric method (Murphy and Riley 1962).

Dissolved organic carbon and nitrogen (DOC and DON) were determined by high-temperature catalytic oxidation using a SHIMADZU TOC-VCPH/CPN analyzer (Jones and Willett 2006). Ammonium nitrogen and nitrate nitrogen (NH + 4-N and NO- 3-N) were determined using a flow analyzer (Chen et al. 2005). Soil microbial biomass carbon, nitrogen, and phosphorus (MBC, MBN, and MBP) were determined by the chloroform fumigation–extraction method (Brookes et al. 1985; Vance et al. 1987), using a SHIMADZU TOC-VCPH/CPN analyzer.

Determination of microbial enzyme activities: One gram of fresh soil was weighed and added to 120 mL of sodium acetate buffer solution, which was then stirred magnetically to form a suspension. In 96-well microplates, 200 μL of the suspension and 50 μL of the substrate solution were added sequentially, mixed thoroughly, and incubated at 25°C in the dark for 4 h. The reaction was terminated by adding 10 μL of 1 mol/L NaOH solution, and fluorescence intensity was measured using a microplate reader at an excitation wavelength of 365 nm and an emission wavelength of 450 nm (Bell et al. 2013; German et al. 2011).

Soil carbon mineralization incubation: Thirty grams of fresh soil were weighed into 70 mL plastic bottles, and soil moisture content was adjusted to 60% of field water holding capacity. The bottles were placed in 1 L sealed jars and incubated in a constant-temperature incubator at 25°C for 49 days. CO_2 emissions were measured on 1, 3, 7, 14, 21, 28, 35, 42, and 49 days of incubation using the alkali absorption method (Chen et al. 2004).

Amplicon sequencing: Soil DNA was extracted using a DNA extraction kit. The V3–V4 hypervariable region of the bacterial 16S rDNA gene was amplified using the forward primer 5'-ACTCCTACGGGAGGCAGCAG-3' and the reverse primer 806R (5'-GGACTACHVGGGTWTCTAAT-3'). The PCR amplification program was as follows: initial denaturation at 95°C for 3 min; denaturation at 95°C for 30 s; annealing at 50°C for 30 s; extension at 72°C for 45 s; 30 cycles in total; followed by a final extension at 72°C for 10 min. Sequencing was performed on the Illumina MiSeq 2500 platform, on which MiSeq paired-end (PE) libraries were constructed and sequenced (Cao et al. 2026).

Data processing and statistical analysis

First-order kinetic equation was used to fit the cumulative soil organic carbon mineralization:

$C_t = C_0(1\text{-}\exp^{-kt})$

where C□ is the cumulative carbon emission from soil after incubation time t; C_0 is the maximum potential carbon emission; k is the rate constant; and t is the incubation time. This equation was used to estimate the maximum potential carbon emission (Zhang et al. 2025).

One-way analysis of variance (One-way ANOVA) was performed using IBM SPSS Statistics 27, and the least significant difference (LSD) test was applied for significance assessment. GraphPad Prism 10.1.2 was used to generate figures for soil carbon mineralization and enzyme activity. Alpha diversity of 16S

rRNA gene sequences was analyzed using MOTHUR (version 1.30.2). Figures for relative abundance of gene sequences, beta diversity, LEfSe analysis, PICRUSt2-based carbon cycling functional prediction and clustering analysis, and Mantel test results were all generated using the Python scientific computing stack, including but not limited to core libraries such as NumPy, Pandas, Matplotlib, Seaborn, and scikit-bio. The partial least squares structural equation model (PLS-SEM) was constructed using the plspm package in R (Cheolho and Sanghoon 2014).

Results and analysis

Effects of different quicklime application rates on soil physicochemical properties

The effects of quicklime application on the physicochemical properties of strongly acidic soils in Chinese fir plantations are presented in Table 1. With increasing quicklime application rates, soil pH showed an overall upward trend; compared with the CK treatment, soil pH values in the T4 and T5 treatments were significantly elevated ($P < 0.05$). Soil organic carbon (SOC), soil microbial biomass carbon (MBC), dissolved organic carbon (DOC), and microbial biomass phosphorus (MBP) all reached their highest levels at the T4 treatment ($P < 0.05$). T5 treatment significantly increased the dissolved organic nitrogen (DON) content and soil ammonium nitrogen (NH + 4-N) content ($P < 0.05$).

Table 1
Soil physicochemical properties of the Chinese fir plantation under different lime application rates

Item	CK	T1	T2	T3	T4	T5
MC	29.46 ± 1.37a	29.98 ± 1.84a	34.94 ± 1.97a	31.21 ± 2.05a	32.04 ± 1.51a	32.54 ± 1.92a
pH	4.71 ± 0.07c	4.76 ± 0.15bc	4.93 ± 0.24abc	5.13 ± 0.29abc	5.25 ± 0.11ab	5.33 ± 0.09a
SOC (g kg^{-1})	12.18 ± 0.50b	13.79 ± 0.74ab	11.97 ± 0.97b	13.51 ± 0.32ab	15.04 ± 1.05a	13.62 ± 0.79ab
TN (g kg^{-1})	0.90 ± 0.00a	1.01 ± 0.13a	0.92 ± 0.12a	1.13 ± 0.27a	1.48 ± 0.32a	1.10 ± 0.19a
TP (g kg^{-1})	0.38 ± 0.05a	0.37 ± 0.05a	0.39 ± 0.08a	0.39 ± 0.06a	0.45 ± 0.06a	0.39 ± 0.03a
MBC (mg kg^{-1})	79.80 ± 6.24bc	56.91 ± 3.96c	86.23 ± 9.99bc	100.57 ± 11.90b	170.74 ± 13.57a	96.95 ± 14.34b
DOC (mg kg^{-1})	171.23 ± 10.86b	183.18 ± 11.02ab	194.62 ± 3.05ab	202.80 ± 7.72ab	216.47 ± 17.43a	191.71 ± 13.20ab
MBN (mg kg^{-1})	24.05 ± 4.53a	24.57 ± 2.67a	24.84 ± 5.38a	26.73 ± 4.81a	32.80 ± 4.42a	25.34 ± 5.66a
DON (mg kg^{-1})	26.03 ± 2.79ab	22.32 ± 4.75ab	22.76 ± 3.83ab	17.62 ± 3.67b	24.39 ± 5.58ab	34.16 ± 4.83a
MBP (mg kg^{-1})	0.69 ± 0.18b	1.06 ± 0.27ab	0.88 ± 0.37ab	1.35 ± 0.55ab	2.02 ± 0.54a	0.94 ± 0.23ab
NH + 4-N (mg kg^{-1})	11.36 ± 1.65ab	7.62 ± 1.22b	9.17 ± 1.56ab	7.70 ± 1.48b	12.09 ± 1.71ab	12.67 ± 1.63a
NO- 3-N (mg kg^{-1})	5.94 ± 0.77a	7.01 ± 1.34a	7.54 ± 1.52a	5.64 ± 0.86a	8.19 ± 1.44a	6.86 ± 0.79a

Note: Data are presented as mean ± standard error (n = 3). Different lowercase letters within the same row indicate significant differences among treatments ($P < 0.05$, LSD test). Abbreviations: CK, control; T1-T5, lime application rates of 375, 750, 1500, 2250, and 3000 $kg \cdot hm^{-2}$, respectively; MC, moisture content; SOC, soil organic carbon; TN, total nitrogen; TP, total phosphorus; MBC, microbial biomass carbon; DOC, dissolved organic carbon; MBN, microbial biomass nitrogen; DON, dissolved organic nitrogen; MBP, microbial biomass phosphorus; NH + 4-N, ammonium nitrogen; NO- 3-N, nitrate nitrogen; The same below.

Effects of different quicklime application rates on soil carbon mineralization

The fitting results of the first-order kinetic model parameters to soil organic carbon mineralization data under different quicklime addition treatments are presented in Table 2. The T4 treatment exhibited the highest potential carbon emission (C_0) ($P < 0.05$), followed by the T1 treatment group, which differed

significantly from the CK, T2, and T3 treatment groups ($P < 0.05$). The dynamic changes in cumulative soil organic carbon mineralization and the variation patterns of soil organic carbon mineralization rates with incubation time under different quicklime addition treatments are shown in Fig. 1. Throughout the entire 49-day incubation period, carbon mineralization in all treatments exhibited the typical characteristic of rapid increase in the early stage followed by gradual stabilization in the later stage. Treatment T4 showed the highest cumulative mineralization, with significant differences relative to all other treatment groups ($P < 0.05$). This was followed by the T5 treatment group, which differed significantly from T3 and CK ($P < 0.05$). Carbon mineralization rates showed an inverse relationship with cumulative mineralization in some treatments. On day 49 of incubation, T4 exhibited the highest mineralization rate, while T5 exhibited the lowest mineralization rate ($P < 0.05$).

Table 2
Kinetic parameters of soil organic carbon mineralization fitted by the first-order kinetic model under different lime application rates

Treatment	Potentially carbon mineralizable (C_0)(mg.kg^{-1})	Constant(K)	Relation coefficient(R^2)
CK	1,158.43 ± 259.01c	0.014 ± 0.004ab	0.999 ± 0.001a
T1	1,728.32 ± 112.90ab	0.010 ± 0.002b	0.999 ± 0.000a
T2	1,056.52 ± 74.38c	0.017 ± 0.003ab	0.997 ± 0.001a
T3	1,045.64 ± 153.30c	0.020 ± 0.003a	0.996 ± 0.004a
T4	1,853.79 ± 131.12a	0.016 ± 0.001ab	0.999 ± 0.000a
T5	1,231.21 ± 246.56bc	0.019 ± 0.005ab	0.998 ± 0.001a

Note: Data are presented as mean ± standard error. Different lowercase letters in the same column indicate significant differences among treatments ($P < 0.05$). C_0, potential carbon mineralization; K, mineralization rate constant; R^2, coefficient of determination.

Note

Error bars represent standard errors (n = 3). Different lowercase letters indicate significant differences among treatments ($P < 0.05$). (a) Cumulative carbon mineralization; (b) Carbon mineralization rate.

Effects of different quicklime application rates on soil enzyme activities

Soil extracellular enzyme activity is an important indicator reflecting soil microbial metabolic capacity and nutrient cycling status. Different quicklime additions produced significant effects on soil enzyme activities (Fig. 2). The activities of β-glucosidase (BG) and cellobiohydrolase (CB) both reached significantly the highest values at the T4 treatment ($P < 0.05$). N-acetyl-β-D-glucosaminidase (NAG) activity under the T4 and T3 treatments was significantly higher than that in the CK, T1, and T2 treatment

groups ($P < 0.05$). Acid phosphatase (ACP) activity under the T4 treatment was significantly higher than that in the T1 and T5 treatment groups ($P < 0.05$).

Note

Error bars represent the standard error of the mean (n = 3). Different letters above the bars indicate significant differences among treatments at $P < 0.05$. (a) β-glucosidase (BG) activity; (b) Cellobiohydrolase (CB) activity; (c) N-acetyl-β-D-glucosaminidase (NAG) activity; (d) Acid phosphatase (ACP) activity.

Soil bacterial β-diversity under different quicklime application rates

PCoA analysis based on Bray-Curtis distances indicated that different lime addition treatments significantly altered soil microbial community structure (PERMANOVA, pseudo-F = 1.768, $P = 0.012$) (Fig. 3). PC1 and PC2 explained 29.59% and 21.88% of community variation, respectively (cumulative 51.47%). The sample distribution in the figure showed that with increasing lime addition (T1 to T5), microbial communities exhibited a pronounced gradient separation trend along the PC1 axis, with the T3, T4, and T5 treatment groups clearly distinguished from the CK and T1 treatment groups in coordinate space.

Note

Different colors represent different lime treatment groups.

Clustering analysis of soil bacterial PICRUSt2 carbon cycling functional predictions under different quicklime application rates

Heatmap analysis based on Z-score normalized abundance data revealed distinct functional clustering patterns among the six treatment groups (CK, T1-T5) (Fig. 4). T2 and CK clustered together, indicating similarity in their functional profiles; whereas T4 and T1 clustered into another group, characterized by an overall reduction in gene abundance.

Carbon fixation pathways exhibited relatively high abundance across all treatments, with the Calvin cycle pathway showing the highest abundance, followed by the reductive TCA cycle and the Wood-Ljungdahl pathway. The overall abundance of methane metabolism-related genes was lower than that of other functional groups. Carbon degradation pathways exhibited the most diverse response patterns. Cellulose degradation genes maintained high abundance, reaching peak values in the T2 treatment. Complex organic matter degradation pathways (including lignin degradation, hemicellulose degradation,

and chitin degradation) showed treatment-specific differences. Fermentation-related genes, particularly mixed acid fermentation, were present at relatively high abundance.

Note

Rows represent different carbon cycling functional pathways, including carbon fixation (C_Fixation), methane metabolism-related (Methane_Metabolism), and carbon degradation (C_Degradation) genes. The color gradient indicates normalized gene abundance (red indicates high abundance, blue indicates low abundance). Dendrograms on the left and top show hierarchical clustering of functional genes and samples, respectively (based on Euclidean distance and Ward's linkage method). Carbon cycling functional pathways include: Calvin cycle, reductive TCA cycle (rTCA cycle), Wood-Ljungdahl pathway, methanogenesis, methane oxidation, cellulose degradation, lignin degradation, hemicellulose degradation, chitin degradation, starch degradation, mixed acid fermentation, and acetate metabolism.

Mantel analysis of soil bacterial community, carbon cycling functional genes, and physicochemical properties

Mantel tests were employed to analyze the correlations among soil physicochemical properties, enzyme activities, carbon mineralization, bacterial community structure, and carbon cycling functional genes (Fig. 5).

Based on Pearson correlation analysis, TN was highly significantly positively correlated with TP, MBC, MBN, and MBP ($P < 0.001$). TP was highly significantly positively correlated with MBN and MBP ($P < 0.001$). The microbial biomass components (MBC, MBN, MBP) were mutually and significantly positively correlated with one another ($P < 0.01$). BG and CB activities were significantly positively correlated ($P < 0.001$), and both were significantly positively correlated with MBC, TN, and MBP ($P < 0.05$). ACP activity was significantly positively correlated with MBP, MBN, TN, and TP ($P < 0.05$).

Mantel test results showed that at the $P < 0.01$ level, NO_3^--N was highly significantly positively correlated with carbon fixation ($P = 0.002$), carbon degradation ($P = 0.003$), and methane metabolism ($P = 0.008$). MBN was likewise highly significantly positively correlated with carbon fixation ($P = 0.008$) and methane metabolism ($P = 0.008$). In addition, a significant positive correlation was found between NAG activity and microbial community structure ($P = 0.004$).

At the $P < 0.05$ level, TP was significantly positively correlated with methane metabolism, carbon fixation, and carbon degradation. MC was significantly positively correlated with carbon degradation and carbon fixation, and its correlation with methane metabolism also reached a significant level. SOC and TN were significantly positively correlated with microbial community structure and the carbon fixation functional module, respectively.

Note

The heatmap displays Pearson correlation coefficients among soil physicochemical properties and enzyme activity indicators (color gradient indicates correlation strength: red for positive, blue for negative). The network diagram on the right shows Mantel test results between environmental factors and microbial community structure (Community) as well as carbon cycling functional modules (C_Fixation, C_Degradation, Methane_Metabolism). Line colors indicate significance levels (orange: $P < 0.01$; green: $0.01 \leq P < 0.05$; gray: $P \geq 0.05$), and line thickness is proportional to the absolute value of Mantel's r (thin: $|r| < 0.1$; medium: $0.1 \leq |r| < 0.2$; thick: $|r| \geq 0.2$). Asterisks in the heatmap denote Pearson correlation significance levels (*$P < 0.05$; **$P < 0.01$; ***$P < 0.001$).

Abbreviations: CMA, cumulative carbon mineralization; MR, mineralization rate.

Partial least squares structural equation modeling (PLS-SEM) analysis

To systematically elucidate the multi-level regulatory mechanisms of quicklime addition on soil carbon mineralization, a partial least squares path model (PLS-PM) comprising 6 latent variables was constructed based on the variable importance in projection (VIP) selection criterion (VIP > 0.8) (Figure 6a). The model contained 21 observed variables, assigned to 6 latent variables: quicklime addition amount (CAO, 1 indicator), soil physicochemical properties (Soil_Properties, 8 indicators), microbial biomass (Microbial_Biomass, 3 indicators), microbial community (Microbial_Community, 4 indicators), enzyme activity (Enzyme_Activity, 4 indicators), and cumulative mineralization (CMA, 1 indicator). The overall model goodness-of-fit (GoF) was 0.5188. The coefficient of determination (R^2) for the target variable cumulative mineralization (CMA) was 0.4062, and the R^2 for enzyme activity (Enzyme_Activity) was 0.5770. The PLS-PM structural model comprised 10 paths in total, of which 5 reached significant levels ($P < 0.05$). Path coefficients and significance test results are presented in Figure 6b, the total effects of each latent variable on enzyme activity and cumulative mineralization are shown in Figure 6c, and the loadings of the latent variables are presented in Figure 6d.

Discussion

Dose-response relationship of quicklime application and the critical threshold for improvement of soil ecological functions

Quicklime addition modified the abiotic soil environment, thereby establishing new boundary conditions for microbial activity. This study identified the T4 treatment as a critical threshold point for the improvement of soil ecological functions. At this dose, soil pH increased from 4.71 to 5.25, that change eliminated the physiological stress imposed by strongly acidic conditions on microorganisms (e.g., aluminum toxicity and proton toxicity) (Singh et al. 2017; Wang et al. 2024; Wang et al. 2021), leading to a striking 192.75% surge in MBP under the T4 treatment. In strongly acidic soils, phosphorus predominantly exists in poorly soluble Fe-P and Al-P forms; when pH rises above 5.0, the degree of protonation on the surfaces of iron and aluminum oxides decreases, promoting phosphate desorption and thereby relieving the phosphorus limitation on microbial growth (Liu et al. 2024; Paradelo et al. 2015). DOC content under the T4 treatment reached 216.47 mg kg^{-1}, representing a 26.42% increase

relative to the control. This change is associated with the increased solubility of soil organic matter driven by pH elevation (Bolan et al. 2011). As a direct energy and carbon source for microorganisms, the increase in DOC provided sufficient substrate for microbial growth. As shown in Table 1, MBC and MBN under the T4 treatment increased by 113.96% and 36.38%, respectively. This observation aligns with Shen (Shen et al. 2025), who reported increases in DOC and microbial biomass following lime application to acidic soils. Favorable pH conditions and elevated carbon availability support microbial biomass accumulation (Aciego Pietri and Brookes 2008; Barcelos et al. 2024).

When the quicklime addition rate was further increased from T4 to T5, despite a marginal pH increase of only 0.08 units (from 5.25 to 5.33), soil microbial biomass declined significantly, with MBC dropping sharply from 170.74 mg kg^{-1} to 96.95 mg kg^{-1} (-43.2%, $P < 0.05$). This result is consistent with the experimental findings of Dumale (Dumale Jr et al. 2011), who reported a declining trend in MBC despite pH increases following liming. We hypothesize that this phenomenon may be attributable to the highest CaO application rate in T5, which upon hydration generated substantially elevated Ca^{2+} concentrations relative to T4. Excessive Ca^{2+} can impair soil nutrient bioavailability through the following mechanisms. (1) Elevated Ca^{2+} concentrations promote the formation of stable Ca-organic matter complexes through calcium bridging, whereby Ca^{2+} coordinates with negatively charged functional groups in soil organic matter (e.g., carboxyl groups $–COO^-$ and phenolic hydroxyl groups $–O^-$) (Han et al. 2025), thereby transferring originally soluble organic carbon from the solution phase to the solid phase and reducing its biological accessibility (Rowley et al. 2018; Rowley et al. 2023). (2) Soil pH is one of the primary determinants of phosphorus speciation and availability (Vengavasi et al. 2021). In acidic soils, phosphorus availability follows an inverted U-shaped response to pH: immobilization by Fe/Al oxides occurs at low pH, while calcium fixation dominates at high pH, with optimal availability in the pH 5.5-6.5 range (Hinsinger 2001). The pH of T4 (5.25) fell within a range sufficient to release phosphorus from Fe/Al-bound forms without triggering calcium phosphate precipitation. Although the pH of T5 exceeded that of T4 by only a marginal increment, the substantially higher Ca^{2+} concentration in T5 is known to lower the precipitation threshold pH, thereby increasing the proportion of phosphorus fixed as calcium phosphate in acidic soils (Amarasiri and Olsen 1973; Hinsinger 2001; Vengavasi et al. 2021). Consistent with this, MBP under T5 declined by 53.5% relative to T4, while TP remained at a comparably low level, indicating reduced phosphorus availability within the system. Pearson correlation analysis revealed that MBC was significantly and positively correlated with both DOC ($r = 0.73$, $P < 0.001$) and MBP ($r = 0.81$, $P < 0.001$), supporting the proposed carbon and phosphorus co-limitation of microbial biomass.

Changes in microbial community structure further supported the resource limitation hypothesis. LEfSe analysis (Figure S3) detected no significantly enriched biomarker taxa under the T5, indicating that the microbial community was in an unstable transitional state and had not yet established a stable dominant population structure. The phylum-level relative abundance profile (Figure S1) showed that the abundances of Acidobacteriota and Verrucomicrobiota declined markedly under T5, while the relative abundance of Proteobacteria surged to 37.96% (+58.1%). Acidobacteriota and Verrucomicrobiota are K-strategists (oligotrophs) that harbor abundant carbohydrate-active enzyme (CAZyme) genes and are capable of degrading complex organic matter (Bergmann et al. 2011; Kielak et al. 2016), whereas

Proteobacteria are predominantly r-strategists (copiotrophs) that preferentially utilize simple carbon sources and have limited extracellular enzyme secretion capacity (Fierer et al. 2007; Goldfarb et al. 2011). Consequently, despite the increase in the relative abundance of Proteobacteria, their small per-cell biomass and functional constraints (Fierer et al. 2007), were insufficient to compensate for the functional loss resulting from the decline of K-strategists, ultimately leading to reductions in total microbial biomass and carbon mineralization function. The PLS-SEM analysis indicated that microbial biomass exerted a strong direct effect on enzyme activity (path coefficient = 0.899, $P < 0.05$), accounting for 80.8% of its variance. Consequently, concurrent community shifts and the observed decline in microbial biomass which driven by multiple pathways , directly impaired soil enzyme activity (Burns et al. 2013).

Decoupling of microbial community structural succession from carbon degradation functional expression following quicklime amendment

High-throughput sequencing revealed a decoupling between functional gene abundance and enzyme activity with increasing quicklime application rates. In T4, the predicted abundance of carbon degradation functional genes (e.g., cellulose and hemicellulose degradation genes) decreased significantly relative to CK (by approximately 29.2%), yet the measured activities of BG and CB reached their highest values across all treatments, increasing by 63.40% and 115.22%, respectively. This divergence indicates a regulatory discrepancy between the genetic potential and actual functional expression of the microbial community. Conventional metagenomic functional prediction tools (e.g., PICRUSt2, Tax4Fun) infer functional gene abundance from 16S rRNA gene abundance (Douglas et al. 2020); however, functional gene abundance does not directly correspond to enzyme activity. A meta-analysis of 415 studies by Rocca (Rocca et al. 2015) demonstrated that only 38% reported a significant positive correlation between functional gene abundance and corresponding process rates, while 62% showed no significant or negative relationships. These findings indicate that gene abundance reflects the functional potential of the microbial community, whereas actual ecosystem functional output is further regulated by transcriptional efficiency, post-translational modifications, enzyme protein stability, and environmental effects on enzyme kinetics.

LEfSe analysis (Figure S3) identified significant enrichment of Verrucomicrobiota in T4, particularly the genus *Candidatus Udaeobacter* (relative abundance increased by 246.19%), along with the order Vicinamibacterales within Acidobacteriota. *Candidatus Udaeobacter* is a characteristically oligotrophic soil bacterium with a streamlined genome (approximately 2-3 Mb) that prioritizes metabolic efficiency over metabolic versatility. This taxon lacks biosynthetic pathways for several amino acids and vitamins, instead relying on environmental acquisition via enriched protease systems and amino acid/peptide transporters, thereby maintaining growth at reduced metabolic cost (Brewer et al. 2016). Members of the order Vicinamibacterales belong to Acidobacteriota subdivision 1, a lineage that is widely distributed and abundant in global soils. Genomic analyses have demonstrated that subdivision 1 members harbor extensive carbohydrate-active enzyme (CAZyme) gene repertoires capable of degrading complex polysaccharides, including cellulose, hemicellulose, and xylan (Eichorst et al. 2018).

Collectively, the elevated enzyme activities observed in T4 are consistent with community succession toward metabolically efficient functional taxa that sustain higher enzyme activity outputs at lower gene abundance levels. This finding suggests that, in the context of soil amendment practices, the metabolic activity and life-history strategies of key functional taxa are more informative indicators of soil carbon cycling capacity than total functional gene abundance or community diversity indices alone (Qian et al. 2026).

Cascading regulation of soil carbon mineralization revealed by PLS-SEM

To quantitatively elucidate the causal relationships among soil physicochemical properties, microbial communities, and carbon mineralization, Mantel tests and PLS-SEM were integrated to construct a comprehensive mechanistic network of driving factors.

Mantel analysis revealed highly significant positive correlations between MBN and carbon fixation (r = 0.270, P = 0.008) and methane metabolism (r = 0.292, P = 0.008), further confirming the pivotal role of microbial biomass nitrogen in regulating soil carbon mineralization (Kuzyakov et al. 2000). The PLS-SEM model demonstrated adequate explanatory power for the observed data (GoF = 0.5188) (Cheolho and Sanghoon 2014). Path analysis identified a sequential cascading regulatory pathway, in which quicklime addition significantly improved soil physicochemical properties (path coefficient = 0.491, $P < 0.05$), which in turn promoted microbial biomass accumulation (path coefficient = 0.860, $P < 0.001$). The resulting increase in microbial biomass subsequently enhanced soil enzyme activity (path coefficient = 0.899, $P < 0.05$), which ultimately drove carbon mineralization (path coefficient = 0.637, $P < 0.01$). These results demonstrate that the effect of quicklime amendment on carbon mineralization is primarily mediated through indirect pathways, operating sequentially through physicochemical amelioration, microbial biomass expansion, and enzymatic activation, rather than through direct physicochemical effects alone.

Carbon pool trade-off effects of quicklime amendment and differentiated application strategies

The mechanistic findings presented above necessitate a critical evaluation of the ecological trade-offs associated with quicklime amendment. While T4 treatment achieved the most substantial improvements in soil pH, nutrient retention, and microbial activity, it concurrently elevated cumulative carbon mineralization by 88.5% relative to CK and reduced the abundance of Calvin cycle functional genes by 28.3%. These observations indicate accelerated depletion of the soil organic carbon pool. First-order kinetic modeling further revealed that the potentially mineralizable carbon fraction in T4 (C_0 = 1,853.792 mg kg^{-1}) accounted for approximately 12.3% of total soil organic carbon, suggesting that sustained high-intensity mineralization without exogenous organic carbon inputs may result in long-term carbon pool deficits.

In contrast, T2 exhibited a more balanced amendment pattern. Despite comparatively modest increases in soil pH and enzyme activity, T2 retained the highest abundance of carbon fixation functional genes (+22.9% relative to CK), with carbon mineralization rates maintained at a moderate level. Mantel analysis revealed a highly significant positive correlation between nitrate nitrogen concentration and the carbon

fixation functional module (r = 0.377, *P* = 0.002), suggesting that low-dose quicklime application sustained a relative equilibrium between autotrophic and heterotrophic microbial communities by promoting nitrification (Kemmitt et al. 2006; Wang et al. 2025), thereby mitigating organic carbon losses.

Based on these findings, differentiated application strategies are proposed according to management objectives: (1) For severely degraded forest soils requiring urgent alleviation of aluminum toxicity and rapid fertility restoration, a single intensive application of T4 (2,250 kg hm^{-2}) may be considered; however, concurrent incorporation of high C/N ratio organic amendments (e.g., straw, wood chips) is essential to offset carbon losses attributable to elevated microbial metabolic activity (Kirkby et al. 2013; Shen et al. 2025), thereby maintaining dynamic carbon pool equilibrium. (2) For sustainable forest land management aimed at maintaining long-term ecological stability and carbon sink function, a phased application strategy of 750-1,500 kg hm^{-2} is recommended. By gently modulating pH, this approach improves the microbial habitat while preserving the carbon sequestration potential of the soil. This progressive amendment mode is more consistent with the long-term sustainability principles of forest ecosystems.

Conclusions

This study integrated soil physicochemical analysis, high-throughput sequencing, and PLS-SEM to investigate the dose-dependent effects of quicklime amendment on carbon cycling in strongly acidic soils of Chinese fir plantations. The following conclusions were drawn:

(1) Quicklime addition exerted nonlinear, threshold-dependent effects on soil carbon cycling. The T4 treatment optimally improved physicochemical conditions, raising soil pH from 4.71 to 5.25, alleviating aluminum toxicity and phosphorus fixation, and increasing microbial biomass carbon and phosphorus by 113.96% and 192.75%, respectively. Exceeding this threshold (T5) reversed these gains, with microbial biomass carbon declining by 43.2%.

(2) Microbial community succession under quicklime amendment was characterized by a shift toward oligotrophic taxa. T4 exhibited a 29.2% decline in carbon degradation gene abundance alongside 63.4% and 115.2% increases in BG and CB enzyme activities, respectively. indicating a decoupling between genetic potential and functional expression.

(3) PLS-SEM analysis revealed a cascading regulatory pathway linking soil physicochemical properties, microbial biomass, enzyme activity, and carbon mineralization. Microbial biomass was identified as the primary driver of enzyme activity (path coefficient = 0.899, $P < 0.05$), explaining 80.8% of its variation.

(4) Quicklime amendment involves a trade-off between soil amelioration and carbon sequestration. Carbon mineralization in T4 increased by 88.5% relative to CK, with potentially mineralizable carbon accounting for 12.3% of SOC, whereas T2 retained the highest carbon fixation gene abundance, suggesting greater carbon sink stability.

These findings suggest that severely degraded forest soils benefit from T4-dose application combined with high C/N ratio organic amendments to mitigate carbon losses, while moderately degraded soils may adopt a phased application strategy of 750-1,500 kg hm^{-2} to balance soil improvement with carbon sink function.

Declarations

Acknowledgements

The work was funded by National Natural Science Foundation of China (32260297), Jiangxi Province Natural Science Foundation of China (20224ACB205003). The authors take this opportunity to thank all for support extended for this study.

References

1. Aciego Pietri JC, Brookes PC (2008) Relationships between soil pH and microbial properties in a UK arable soil. Soil Biol Biochem 40:1856–1861. https://doi.org/10.1016/j.soilbio.2008.03.020
2. Ahmad W, Singh B, Dijkstra FA, Dalal RC, Geelan-Small P (2014) Temperature sensitivity and carbon release in an acidic soil amended with lime and mulch. Geoderma 214–215:168–176. https://doi.org/10.1016/j.geoderma.2013.09.014
3. Amarasiri SL, Olsen SR (1973) Liming as Related to Solubility of P and Plant Growth in an Acid Tropical Soil. Soil Sci Soc Am J 37:716–721. https://doi.org/10.2136/sssaj1973.03615995003700050026x
4. Barcelos JPQ, Sánchez-Rodríguez AR, Bargiela R, Mariano E, Gloyshina OV, Jones DL, Rosolem CA (2024) Lime, gypsum, and nitrogen as drivers to increase the abundance of soil fungi and N-cycling microorganisms in integrated agricultural systems. Appl Soil Ecol 202:105549. https://doi.org/10.1016/j.apsoil.2024.105549
5. Bell CW, Fricks BE, Rocca JD, Steinweg JM, McMahon SK, Wallenstein MD (2013) High-throughput Fluorometric Measurement of Potential Soil Extracellular Enzyme Activities. J Visualized Experiments 81:e50961. https://doi.org/10.3791/50961
6. Bergmann GT, Bates ST, Eilers KG, Lauber CL, Caporaso JG, Walters WA, Knight R, Fierer N (2011) The under-recognized dominance of Verrucomicrobia in soil bacterial communities. Soil Biol Biochem 43:1450–1455. https://doi.org/10.1016/j.soilbio.2011.03.012
7. Błońska E, Lasota J, Gruba P (2016) Effect of temperate forest tree species on soil dehydrogenase and urease activities in relation to other properties of soil derived from loess and glaciofluvial sand. Ecol Res 31:655–664. https://doi.org/10.1007/s11284-016-1375-6
8. Bolan NS, Adriano DC, Kunhikrishnan A, James T, McDowell R, Senesi N (2011) Chapter One - Dissolved Organic Matter: Biogeochemistry, Dynamics, and Environmental Significance in Soils. Adv Agron 110:1–75. https://doi.org/10.1016/B978-0-12-385531-2.00001-3

9. Bremner JM (1996) Nitrogen-Total. Methods of Soil Analysis. https://doi.org/10.2136/sssabookser5.3.c37
10. Brewer TE, Handley KM, Carini P, Gilbert JA, Fierer N (2016) Genome reduction in an abundant and ubiquitous soil bacterium 'Candidatus Udaeobacter copiosus'. Nat Microbiol 2:16198. https://doi.org/10.1038/nmicrobiol.2016.198
11. Brookes PC, Landman A, Pruden G, Jenkinson DS (1985) Chloroform fumigation and the release of soil nitrogen: A rapid direct extraction method to measure microbial biomass nitrogen in soil. Soil Biol Biochem 17:837–842. https://doi.org/10.1016/0038-0717(85)90144-0
12. Burns RG, DeForest JL, Marxsen J, Sinsabaugh RL, Stromberger ME, Wallenstein MD, Weintraub MN, Zoppini A (2013) Soil enzymes in a changing environment: Current knowledge and future directions. Soil Biol Biochem 58:216–234. https://doi.org/10.1016/j.soilbio.2012.11.009
13. Cao Y, Chen Z, Li Y, Xu S, Yang C, Wu Z, Liu B, Zhang C, Liu D, Yin B, Ding W (2026) Soil multifunctionality driven by shift of bacterial rather than fungal community promotes cropland productivity via enhancing nitrogen use efficiency. Appl Soil Ecol 218:106721. https://doi.org/10.1016/j.apsoil.2025.106721
14. Chen CR, Xu ZH, Keay P, Zhang SL (2005) Total soluble nitrogen in forest soils as determined by persulfate oxidation and by high temperature catalytic oxidation. Aust J Soil Res 43:515–523. https://doi.org/10.1071/SR04132
15. Chen CR, Xu ZH, Mathers NJ (2004) Soil Carbon Pools in Adjacent Natural and Plantation Forests of Subtropical Australia. Soil Sci Soc Am J 68:282–291. https://doi.org/10.2136/sssaj2004.2820
16. Cheolho Y, Sanghoon K (2014) A Tutorial on PLS Structural Equating Modeling using R: (Centering on) Exemplified Research Model and Data. Inform Syst Rev 16:89–112. https://dx.doi.org/10.14329/isr.2014.16.3.089
17. Douglas GM, Maffei VJ, Zaneveld JR, Yurgel SN, Brown JR, Taylor CM, Huttenhower C, Langille MGI (2020) PICRUSt2 for prediction of metagenome functions. Nat Biotechnol 38:685–688. https://doi.org/10.1038/s41587-020-0548-6
18. Dumale WA Jr, Miyazaki T, Hirai K, Nishimura T (2011) SOC Turnover and Lime-CO_2 Evolution during Liming of an Acid Andisol and Ultisol. Open J Soil Sci 01:49–53. https://doi.org/10.4236/ojss.2011.12007
19. Eichorst SA, Trojan D, Roux S, Herbold C, Rattei T, Woebken D (2018) Genomic insights into the Acidobacteria reveal strategies for their success in terrestrial environments. Environ Microbiol 20:1041–1063. https://doi.org/10.1111/1462-2920.14043
20. Fageria NK, Baligar VC (2008) Chap. 7 Ameliorating Soil Acidity of Tropical Oxisols by Liming For Sustainable Crop Production. Adv Agron 99:345–399. https://doi.org/10.1016/S0065-2113(08)00407-0
21. Fierer N, Bradford MA, Jackson RB (2007) TOWARD AN ECOLOGICAL CLASSIFICATION OF SOIL BACTERIA. Ecology 88:1354–1364. https://doi.org/10.1890/05-1839

22. German D, Weintraub M, Grandy S, Lauber C, Rinkes Z, Allison S (2011) Optimization of hydrolytic and oxidative enzyme methods for ecosystem studies. Soil Biol Biochem 43:1387–1397. https://doi.org/10.1016/j.soilbio.2011.03.017
23. Goldfarb KC, Karaoz U, Hanson CA, Santee CA, Bradford MA, Treseder KK, Wallenstein MD, Brodie EL (2011) Differential Growth Responses of Soil Bacterial Taxa to Carbon Substrates of Varying Chemical Recalcitrance. Front Microbiol 2:e00094. https://doi.org/10.3389/fmicb.2011.00094
24. Grover SP, Butterly CR, Wang X, Tang C (2017) The short-term effects of liming on organic carbon mineralisation in two acidic soils as affected by different rates and application depths of lime. Biol Fertil Soils 53:431–443. https://doi.org/10.1007/s00374-017-1196-y
25. Han Z, Li S, Degré A, Gao H, Zheng F, Song X, Jia A, Wu X (2025) Conservation tillage and wheat straw managements improve soil organic carbon sequestration via calcium-mediated microbial communities and aggregate stability in Calcaric Cambisols. J Environ Manage 396:128182. https://doi.org/10.1016/j.jenvman.2025.128182
26. He D, Ou Y, Dong Z, Zhu B (2025) Industrial by-products as alternative additives for mitigating soil acidification and improving crop yield via immobilizing soil exchangeable Al^{3+} and restructuring microbial community. J Environ Chem Eng 13:119678. https://doi.org/10.1016/j.jece.2025.119678
27. Hinsinger P (2001) Bioavailability of soil inorganic P in the rhizosphere as affected by root-induced chemical changes: a review. Plant Soil 237:173–195. https://doi.org/10.1023/A:1013351617532
28. Holland JE, Bennett AE, Newton AC, White PJ, McKenzie BM, George TS, Pakeman RJ, Bailey JS, Fornara DA, Hayes RC (2018) Liming impacts on soils, crops and biodiversity in the UK: A review. Sci Total Environ 610–611:316–332. https://doi.org/10.1016/j.scitotenv.2017.08.020
29. Ismail N, Khiari L, Daoud R (2026) Calcium amendment strategies for alfalfa with biomass yield responses across contrasting soils and stand types. Field Crops Res 339:110347. https://doi.org/10.1016/j.fcr.2026.110347
30. Jones D, Willett V (2006) Experimental evaluation of methods to quantify dissolved organic nitrogen (DON) and dissolved organic carbon (DOC) in soil. Soil Biol Biochem 38:991–999. https://doi.org/10.1016/j.soilbio.2005.08.012
31. Jouichat H, Khiari L (2026) Reconstructing soil acidity neutralization curves using Machine learning and chemical or spectral soil signatures. Geoderma 465:117645. https://doi.org/10.1016/j.geoderma.2025.117645
32. Jouichat H, Khiari L, Gallichand J, Ismail M (2024) Modeling temporal variation of soil acidity after the application of liming materials. Soil Tillage Res 240:106050. https://doi.org/10.1016/j.still.2024.106050
33. Kemmitt SJ, Wright D, Goulding KWT, Jones DL (2006) pH regulation of carbon and nitrogen dynamics in two agricultural soils. Soil Biol Biochem 38:898–911. https://doi.org/10.1016/j.soilbio.2005.08.006
34. Kielak AM, Barreto CC, Kowalchuk GA, van Veen JA, Kuramae EE (2016) The Ecology of Acidobacteria: Moving beyond Genes and Genomes. Front Microbiol 7:744.

https://doi.org/10.3389/fmicb.2016.00744

35. Kirkby CA, Richardson AE, Wade LJ, Batten GD, Blanchard C, Kirkegaard JA (2013) Carbon-nutrient stoichiometry to increase soil carbon sequestration. Soil Biol Biochem 60:77–86. https://doi.org/10.1016/j.soilbio.2013.01.011
36. Kuzyakov Y, Friedel J, Stahr K (2000) Review of mechanisms and quantification of priming effects. Soil Biol Biochem 32:1485–1498. https://doi.org/10.1016/S0038-0717(00)00084-5
37. Lei Y, Li J, Cai Z, Sun N, Wu L, He X, Xu M (2026) Soil acidification promotes bacterial wilt: Meta-analysis reveals key modulators and management strategies via pH and available phosphorus. Agricultural Environ Sustain 1:100003. https://doi.org/10.1016/j.ages.2025.100003
38. Li Z, Gao X, Li D, Gao J, Li J, Cai Z, Sun N, Wu L, Xu M (2025) Differential responses of bacteria, fungi, and C, N, P functions to soil acidification in farmland: A meta-analysis. Environ Technol Innov 40:104499. https://doi.org/10.1016/j.eti.2025.104499
39. Liu X, Zhang Y, Wang Z, Chen Z (2024) The contribution of organic and chemical fertilizers on the pools and availability of phosphorus in agricultural soils based on a meta-analysis. Eur J Agron 156:127144. https://doi.org/10.1016/j.eja.2024.127144
40. Murphy J, Riley JP (1962) A modified single solution method for the determination of phosphate in natural waters. Anal Chim Acta 27:31–36. https://doi.org/10.1016/S0003-2670(00)88444-5
41. Nelson DW, Sommers LE (1996) Total Carbon, Organic Carbon, and Organic Matter. Methods Soil Anal 961–1010. https://doi.org/10.2136/sssabookser5.3.c34
42. Paradelo R, Virto I, Chenu C (2015) Net effect of liming on soil organic carbon stocks: A review. Agric Ecosyst Environ 202:98–107. https://doi.org/10.1016/j.agee.2015.01.005
43. Qian R, Gao L, Liu J, Biswas A, Peng X (2026) Linking microbial life strategies to carbon mineralization under diverse tillage practices: Insights from eroding black soil hillslopes. Agric Ecosyst Environ 399:110174. https://doi.org/10.1016/j.agee.2025.110174
44. Rocca JD, Hall EK, Lennon JT, Evans SE, Waldrop MP, Cotner JB, Nemergut DR, Graham EB, Wallenstein MD (2015) Relationships between protein-encoding gene abundance and corresponding process are commonly assumed yet rarely observed. ISME J 9:1693–1699. https://doi.org/10.1038/ismej.2014.252
45. Rowley MC, Grand S, Verrecchia ÉP (2018) Calcium-mediated stabilisation of soil organic carbon. Biogeochemistry 137:27–49. https://doi.org/10.1007/s10533-017-0410-1
46. Rowley MC, Nico PS, Bone SE, Marcus MA, Pegoraro EF, Castanha C, Kang K, Bhattacharyya A, Torn MS, Peña J (2023) Association between soil organic carbon and calcium in acidic grassland soils from Point Reyes National Seashore, CA. Biogeochemistry 165:91–111. https://doi.org/10.1007/s10533-023-01059-2
47. Selvaraj S, Duraisamy V, Huang Z, Guo F, Ma X (2017) Influence of long-term successive rotations and stand age of Chinese fir (*Cunninghamia lanceolata*) plantations on soil properties. Geoderma 306:127–134. https://doi.org/10.1016/j.geoderma.2017.07.014

48. Shen Z, Liu K, Li J, Daba NA, Alam MA, Tadesse KA, Han T, Zhang H (2025) Optimal lime materials for mitigating global warming potential with and without straw application in acidic upland soil. Environ Science: Processes Impacts 27:3420–3430. https://doi.org/10.1039/d5em00494b
49. Singh S, Tripathi DK, Singh S, Sharma S, Dubey NK, Chauhan DK, Vaculík M (2017) Toxicity of aluminium on various levels of plant cells and organism: A review. Environ Exp Bot 137:177–193. https://doi.org/10.1016/j.envexpbot.2017.01.005
50. Vance ED, Brookes PC, Jenkinson DS (1987) An extraction method for measuring soil microbial biomass C. Soil Biol Biochem 19:703–707. https://doi.org/10.1016/0038-0717(87)90052-6
51. Vengavasi K, Pandey R, Soumya PR, Hawkesford MJ, Siddique KHM (2021) Below-ground physiological processes enhancing phosphorus acquisition in plants. Plant Physiol Rep 26:600–613. https://doi.org/10.1007/s40502-021-00627-8
52. Wang J, Duan Y, Li G, Zhang L, Li D, Liu K, Cui Xa, Zhou B, Gao H, Han X, Ma J, Liu S, Huang S, Zhang A, Hua K, Wang J, Rui Y, Zhang W (2024) Response of soil gross nitrogen mineralization to fertilization practices in China's uplands. J Clean Prod 480:144123. https://doi.org/10.1016/j.jclepro.2024.144123
53. Wang J, Huang Q, Yu D, Zhang Y, Uwiragiye Y, Fallah N, Chen M, Cheng Y (2025) Effectiveness of Nitrification Inhibitor in Reducing N_2O Emissions Depends on Soil Acidification Mitigation in Acid Soils. Agronomy 15:1536. https://doi.org/10.3390/agronomy15071536
54. Wang Q, Wang S, Yu X (2011) Decline of soil fertility during forest conversion of secondary forest to Chinese fir plantations in subtropical China. Land Degrad Dev 22:444–452. https://doi.org/10.1002/ldr.1030
55. Wang Y, Yao Z, Zhan Y, Zheng X, Zhou M, Yan G, Wang L, Werner C, Butterbach-Bahl K (2021) Potential benefits of liming to acid soils on climate change mitigation and food security. Glob Change Biol 27:2807–2821. https://doi.org/10.1111/gcb.15607
56. Yang X, Ma D, Yang T, Zhang Y, Chen L, Jiang H, Chen B, Zhang N, Zou H, Zhang C, Zhou G, Zhou Y, Zhang J (2026) Dual mechanisms of mineral-microbial interactions in suppressing organic carbon sequestration in calcareous soils. J Environ Manage 400:128692. https://doi.org/10.1016/j.jenvman.2026.128692
57. Zhang J, Wang F, Yang J, Zhang Y, Qiu L, Chen Z, Wang X, Zhang T, Li S, Tong J, Lu S, Zhang Y (2025) The Effects of Tree Species on Soil Organic Carbon Mineralization in Reservoir Water-Level Drawdown Zones. Forests 16:1145. https://doi.org/10.3390/f16071145

Figures

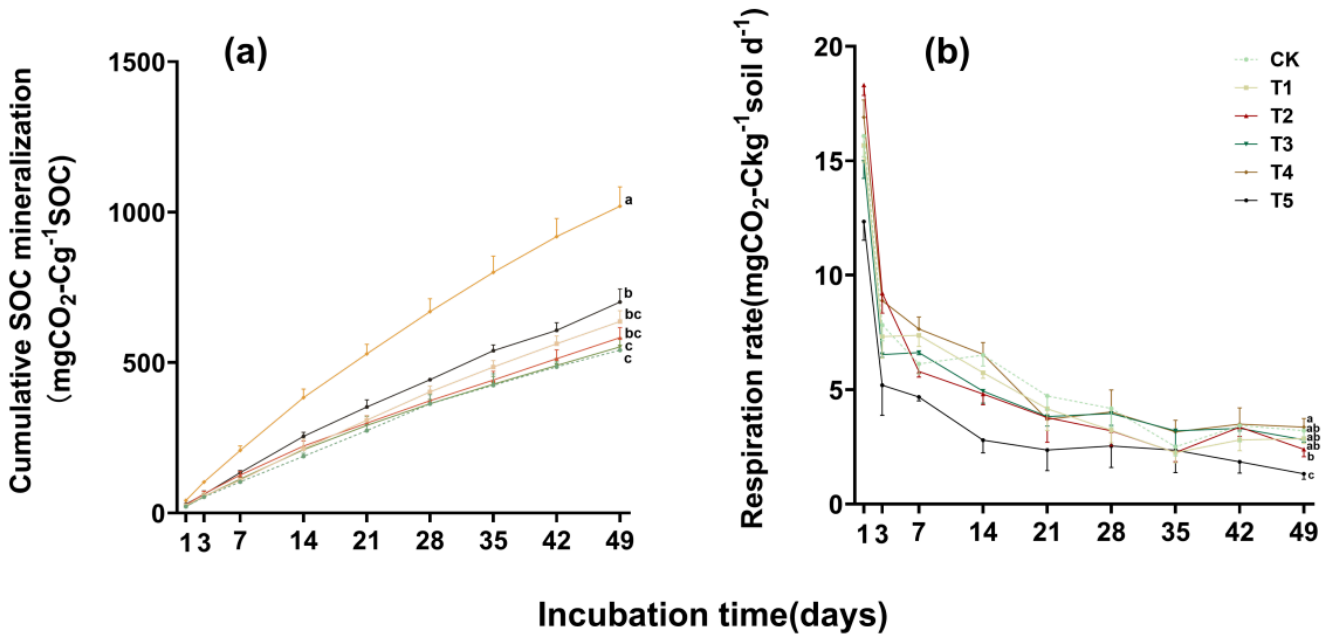

Figure 1

Dynamics of cumulative soil organic carbon mineralization and mineralization rates under different lime application rates

Note: Error bars represent standard errors (n=3). Different lowercase letters indicate significant differences among treatments ($P < 0.05$). (a) Cumulative carbon mineralization; (b) Carbon mineralization rate.

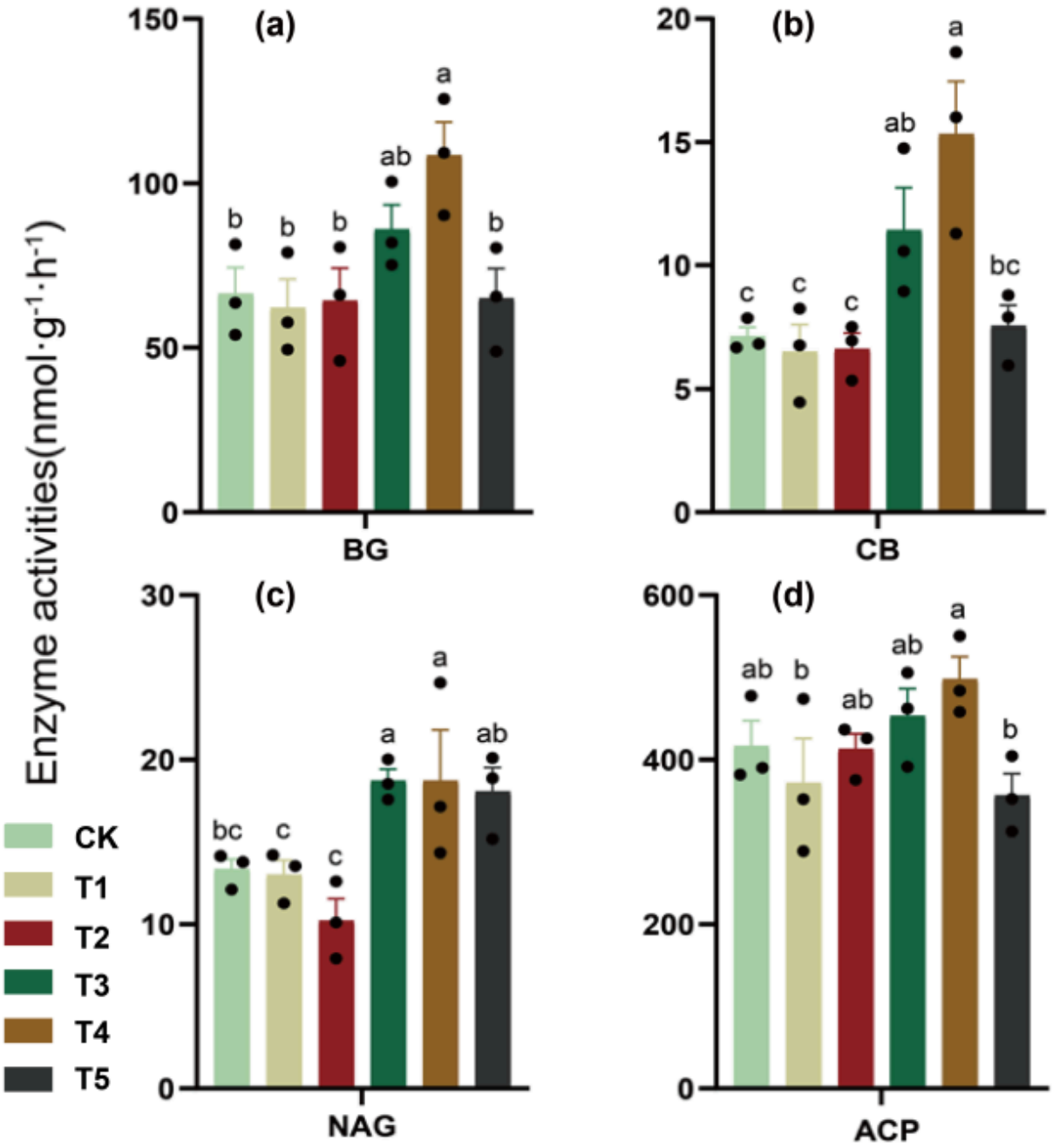

Figure 2

Effects of different quicklime addition rates on soil extracellular enzyme activities

Note: Error bars represent the standard error of the mean (n=3). Different letters above the bars indicate significant differences among treatments at $P < 0.05$. (a) β-glucosidase (BG) activity; (b)

Cellobiohydrolase (CB) activity; (c) N-acetyl-β-D-glucosaminidase (NAG) activity; (d) Acid phosphatase (ACP) activity.

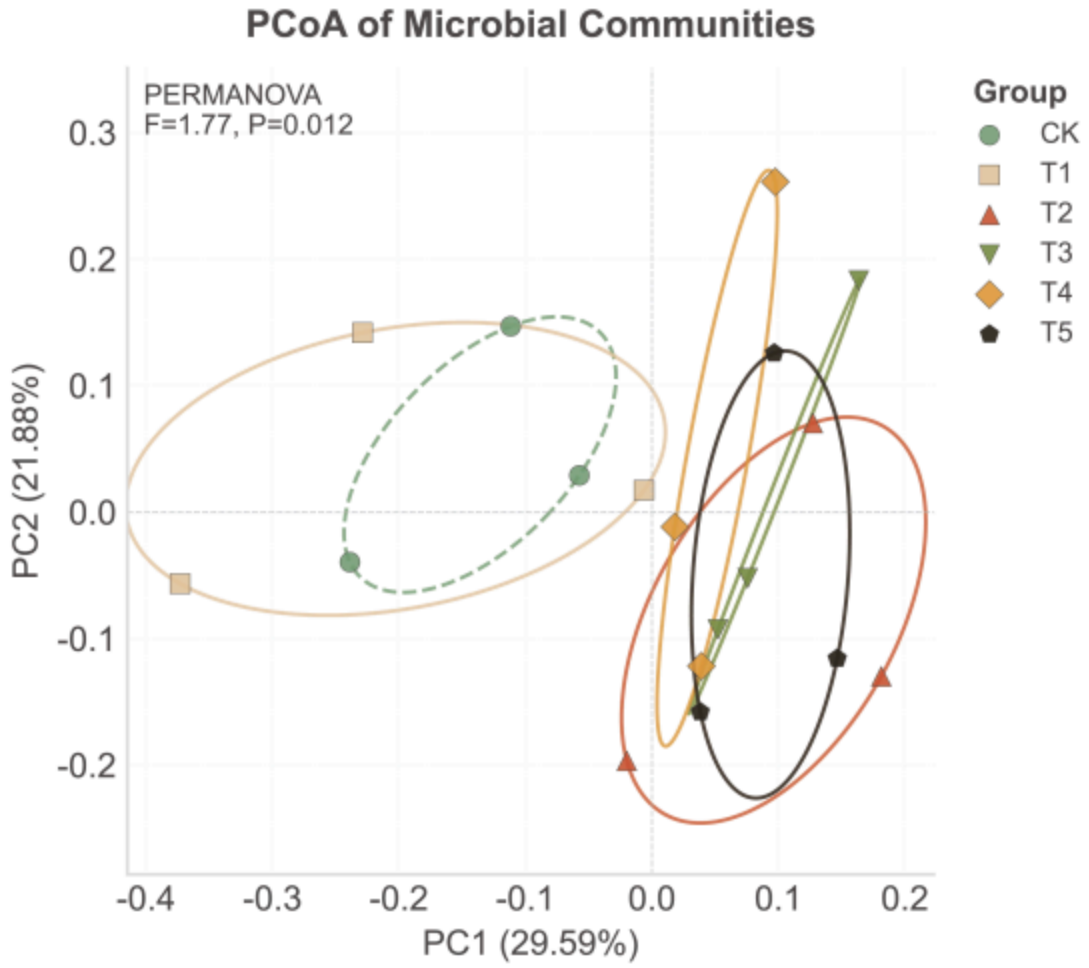

Figure 3

Principal Coordinate Analysis (PCoA) of soil bacterial communities based on Bray-Curtis distances under different lime application rates

Note: Different colors represent different lime treatment groups.

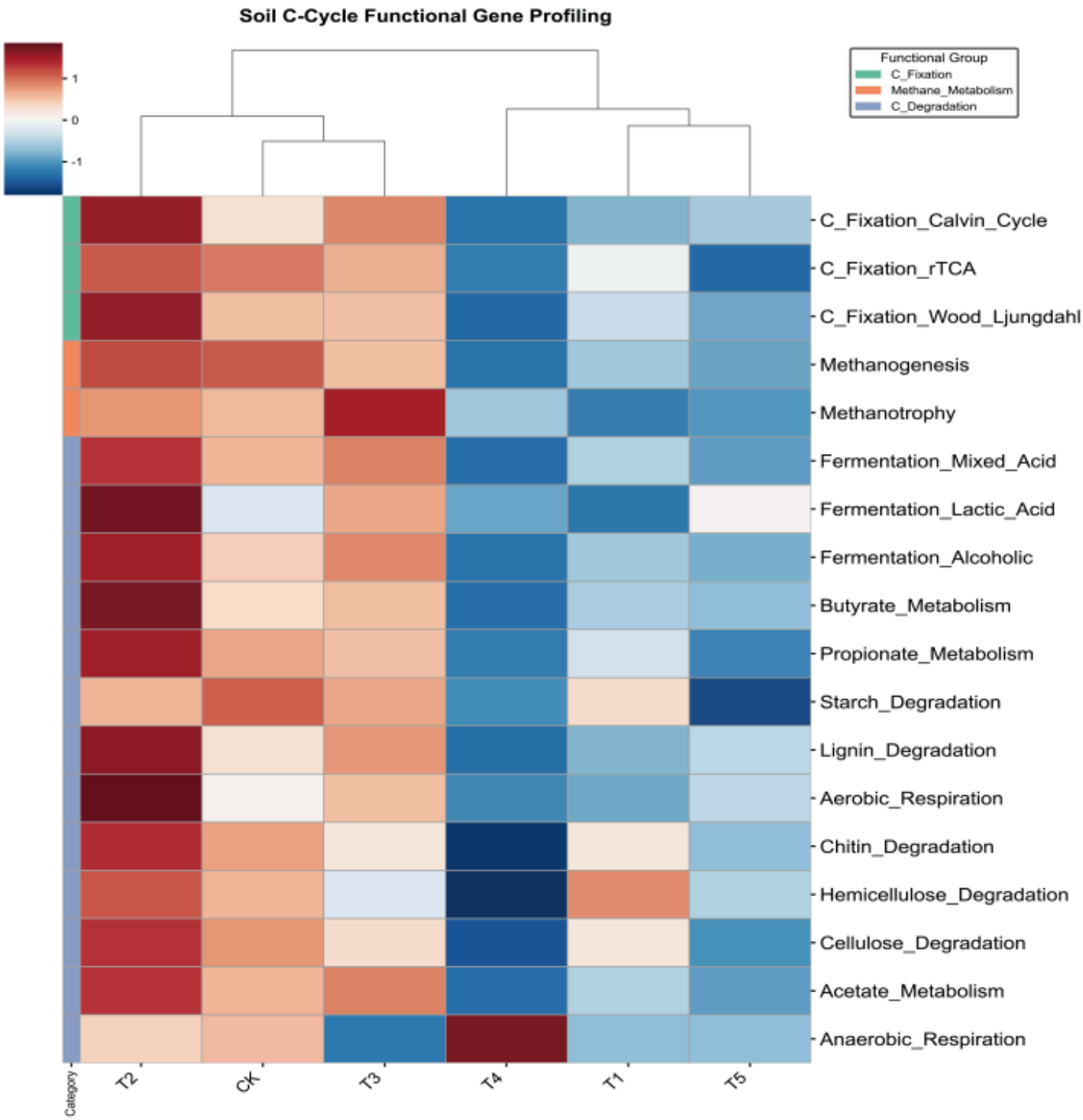

Figure 4

Hierarchical clustering heatmap of carbon cycling functional gene abundance in soil bacteria under different quicklime application rates

Note: Rows represent different carbon cycling functional pathways, including carbon fixation (C_Fixation), methane metabolism-related (Methane_Metabolism), and carbon degradation (C_Degradation) genes. The color gradient indicates normalized gene abundance (red indicates high abundance, blue indicates low abundance). Dendrograms on the left and top show hierarchical clustering of functional genes and samples, respectively (based on Euclidean distance and Ward's

linkage method). Carbon cycling functional pathways include: Calvin cycle, reductive TCA cycle (rTCA cycle), Wood-Ljungdahl pathway, methanogenesis, methane oxidation, cellulose degradation, lignin degradation, hemicellulose degradation, chitin degradation, starch degradation, mixed acid fermentation, and acetate metabolism.

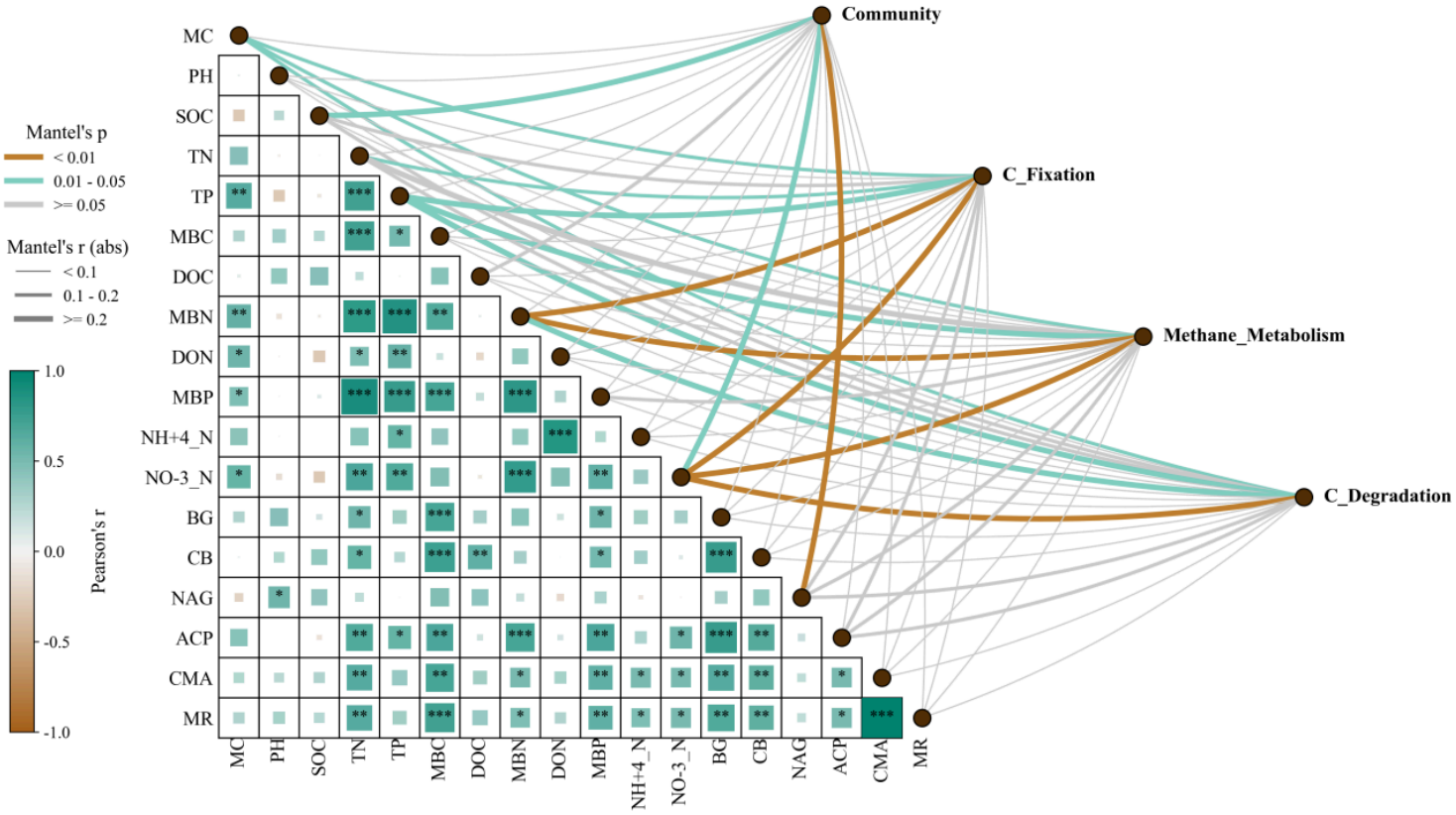

Figure 5

Mantel test correlations linking soil physicochemical properties, bacterial community structure, and carbon cycling functional genes

Note: The heatmap displays Pearson correlation coefficients among soil physicochemical properties and enzyme activity indicators (color gradient indicates correlation strength: red for positive, blue for negative). The network diagram on the right shows Mantel test results between environmental factors and microbial community structure (Community) as well as carbon cycling functional modules (C_Fixation, C_Degradation, Methane_Metabolism). Line colors indicate significance levels (orange: $P < 0.01$; green: $0.01 \le P < 0.05$; gray: $P \ge 0.05$), and line thickness is proportional to the absolute value of Mantel's r (thin: $|r| < 0.1$; medium: $0.1 \le |r| < 0.2$; thick: $|r| \ge 0.2$). Asterisks in the heatmap denote Pearson correlation significance levels (*$P < 0.05$; **$P < 0.01$; ***$P < 0.001$).

Abbreviations: CMA, cumulative carbon mineralization; MR, mineralization rate.

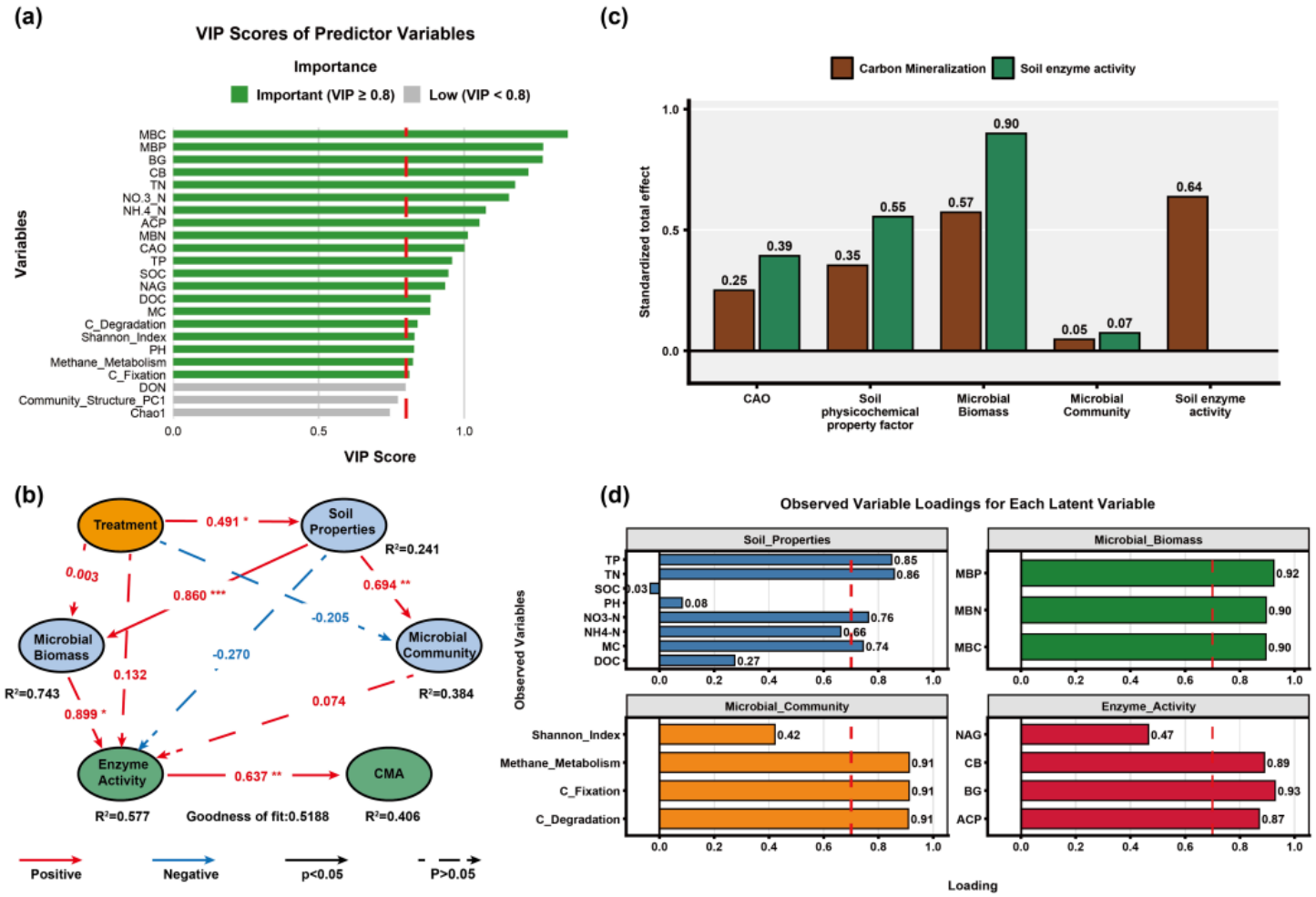

Figure 6

Partial least squares path modeling (PLS-PM) revealing the multi-stage driving mechanisms of soil carbon mineralization under lime application

Note: (a) Variable Importance in Projection (VIP) scores used to select key predictors for the model (VIP > 0.8).

(b) The structural path diagram of the PLS-PM. Red and blue arrows indicate positive and negative effects, respectively; solid and dashed lines denote significant ($P < 0.05$) and non-significant path coefficients, respectively. Numbers adjacent to arrows represent standardized path coefficients, *$P <$ 0.05; **$P < 0.01$; ***$P < 0.001$. R^2 values indicate the proportion of variance explained for endogenous latent variables (enzyme activity and cumulative mineralization). GoF (0.5188) represents the overall Goodness of Fit.

(c) Standardized total effects (sum of direct and indirect effects) of latent variables on cumulative soil organic carbon mineralization and enzyme activity.

(d) Outer loadings of observed variables for their respective latent variables.

Abbreviations: CAO, lime application rate; Soil_Properties, soil physicochemical properties; Microbial_Biomass, microbial biomass; Microbial_Community, microbial community (including diversity indices and carbon cycling functional gene abundances); Enzyme_Activity, extracellular enzyme activity; CMA, cumulative carbon mineralization.